

Iterative linearized density matrix propagation for modeling coherent excitation energy transfer in photosynthetic light harvesting

Cite as: J. Chem. Phys. **133**, 184108 (2010); <https://doi.org/10.1063/1.3498901>

Submitted: 08 July 2010 . Accepted: 18 September 2010 . Published Online: 11 November 2010

P. Huo, and D. F. Coker



View Online



Export Citation

ARTICLES YOU MAY BE INTERESTED IN

[Communication: Partial linearized density matrix dynamics for dissipative, non-adiabatic quantum evolution](#)

The Journal of Chemical Physics **135**, 201101 (2011); <https://doi.org/10.1063/1.3664763>

[Unified treatment of quantum coherent and incoherent hopping dynamics in electronic energy transfer: Reduced hierarchy equation approach](#)

The Journal of Chemical Physics **130**, 234111 (2009); <https://doi.org/10.1063/1.3155372>

[Perspective: Nonadiabatic dynamics theory](#)

The Journal of Chemical Physics **137**, 22A301 (2012); <https://doi.org/10.1063/1.4757762>

Lock-in Amplifiers

Find out more today



Zurich
Instruments



Iterative linearized density matrix propagation for modeling coherent excitation energy transfer in photosynthetic light harvesting

P. Huo¹ and D. F. Coker^{1,2,a)}

¹*Department of Chemistry, Boston University, 590 Commonwealth Avenue, Boston, Massachusetts 02215, USA*

²*Department of Physics, University College Dublin, Dublin 4, Ireland*

(Received 8 July 2010; accepted 18 September 2010; published online 11 November 2010)

Rather than incoherent hopping between chromophores, experimental evidence suggests that the excitation energy transfer in some biological light harvesting systems initially occurs coherently, and involves coherent superposition states in which excitation spreads over multiple chromophores separated by several nanometers. Treating such delocalized coherent superposition states in the presence of decoherence and dissipation arising from coupling to an environment is a significant challenge for conventional theoretical tools that either use a perturbative approach or make the Markovian approximation. In this paper, we extend the recently developed iterative linearized density matrix (ILDm) propagation scheme [E. R. Dunkel *et al.*, *J. Chem. Phys.* **129**, 114106 (2008)] to study coherent excitation energy transfer in a model of the Fenna–Matthews–Olsen light harvesting complex from green sulfur bacteria. This approach is nonperturbative and uses a discrete path integral description employing a short time approximation to the density matrix propagator that accounts for interference between forward and backward paths of the quantum excitonic system while linearizing the phase in the difference between the forward and backward paths of the environmental degrees of freedom resulting in a classical-like treatment of these variables. The approach avoids making the Markovian approximation and we demonstrate that it successfully describes the coherent beating of the site populations on different chromophores and gives good agreement with other methods that have been developed recently for going beyond the usual approximations, thus providing a new reliable theoretical tool to study coherent exciton transfer in light harvesting systems. We conclude with a discussion of decoherence in independent bilinearly coupled harmonic chromophore baths. The ILDM propagation approach in principle can be applied to more general descriptions of the environment. © 2010 American Institute of Physics. [doi:10.1063/1.3498901]

I. INTRODUCTION

Photosynthetic systems such as the various well studied bacterial models^{1–11} involve assemblies of many bacteriochlorophyll molecules, for example, arrayed in structured complexes embedded in protein scaffoldings. These ubiquitous structures have evolved to function as extraordinarily efficient solar energy capture, and transfer systems that funnel electronic excitation into reaction centers where long term energy storage is initiated. Remarkably, recent multidimensional nonlinear spectroscopic experiments¹² have demonstrated that the dominant energy transport pathways in these systems are determined by the spatial characteristics of the excited state wave functions of the *entire* complex, which can involve many tens of electronically coupled chromophores spread over large regions of space. Experiments reveal that in the early stages of the excitation energy transfer in these nanoscale energy “transmission grids,” the process involves quantum coherent superposition of states that manifests itself, at least at early times in observed quantum beats among the excitonic states involved in the energy transfer processes.¹² Even more surprising is the recent find-

ing that the protein scaffolding that supports the chromophores seems to move in a collective fashion producing correlated fluctuation in the energy levels of the different chromophores and effectively protecting the excitonic coherence.¹³ Exactly what role, if any, this fundamentally quantum behavior plays in the functioning of these structures is as yet unclear, but many imaginative suggestions have been made.^{12–16} Reliable simulation methods that can treat many coupled chromophores interacting with a nanostructured collective bath are required to address these intriguing questions and the goal of the studies described here is to explore the accuracy of several approaches that are, in principle, capable of addressing such questions.

Until very recently, the energy transfer mechanism in these systems has usually been treated theoretically using either Förster resonance energy transfer (FRET) theory^{17–21} or the Redfield equation.^{22,23} The FRET rate expression is valid when the electronic coupling between chromophores is small compared to the electronic-phonon coupling, and the approach uses a perturbative treatment of the electronic coupling and assumes incoherent hopping of the exciton between a single donor and acceptor. To overcome the limitation of this theory, Jang *et al.*^{17,18,24–26} developed a

^{a)}Electronic mail: coker@bu.edu.

multichromophore version that incorporates interference between transfer pathways involving multiple donors and acceptors. The Redfield equation, on the other hand, is valid when the electron-phonon coupling is small compared to the electronic coupling between chromophores, and uses perturbation theory to treat the electron-phonon coupling, and integrates or projects out the bath degree of freedom to obtain a reduced master equation for density matrix evolution in the Markovian approximation. In most typical situations in photosynthetic systems, the solvent reorganization energy is not small compared with the electronic coupling, which leads to an inaccurate treatment by perturbation theory. Also the Markovian approximation that requires phonon excitations to relax to thermal equilibrium instantaneously is often a poor approximation in these systems as the phonon characteristic relaxation time scale is normally quite long. Moreover, the propagation of the diagonal element of the reduced density matrix in this approximation sometimes violates positivity for low temperatures. The Lindblad equation,^{27–30} which is commonly used, adds the secular approximation to the Redfield equation to guarantee positive definite populations. This secular approximation separates the dynamics of the evolution of the populations and coherences,³⁰ and also simplifies the numerical calculation. However, since the secular approximation eliminates some of the relaxation terms it can lead to an inappropriate treatment of interactions between the chromophores and their phonon bath.

To go beyond the perturbative treatment and Markov approximations, Ishizaki *et al.*^{15,31,32} extended a nonperturbative hierarchical reduced master equation approach. By incorporating many auxiliary variables, this type of method can describe the coherent beating of the exciton amplitudes in multichromophore systems for much longer, and over a wider range of parameters than the conventional Redfield equations. The applicability of the approach is restricted by the underlying model it assumes, and the approximations that must be made such as the following: the bilinear approximation to the generally complex nature of the system-bath interactions, the overdamped Brownian oscillator, and Gaussian random noise models. Chakraborty *et al.*,³³ using a non-Markovian quantum jump (NMQJ) approach,^{34,35} together with a time convolutionless (TCL) equation, found that non-Markovian effects are crucial for preserving the coherent behavior of the excitation energy transfer. Jang *et al.*^{36,37} developed another type of the reduced equation that is based on a small polaron transformation. The main advantage of all these reduced descriptions is that they analytically integrate, or project out the bath degrees of freedom, and incorporate their influence by the time nonlocality of the memory kernel without having to treat the evolution of the bath degrees of freedom explicitly. The disadvantage is trying to find reliable ways to capture the effect of the time nonlocality of the memory kernel, which usually requires considerable effort, for example using large numbers of auxiliary variables³² that can substantially increase the computational complexity of such calculations.

Rather than using a reduced description, a full calculation including both electronic and nuclear degrees of freedom is possible if one can justify employing a mixed

quantum-classical or semiclassical description of the dynamics that treats the electronic part quantum mechanically, while the nuclear degrees of freedom are described classically or semiclassically. Recently, Tao and Miller³⁸ used the linearized semiclassical Initial value representation (LSC-IVR) Path integral method together with Meyer–Miller–Stock–Thoss “mapping Hamiltonian” description^{39–42} for the electronic degrees of freedom (which are also linearized in their approach) to study the coherent exciton transfer in a model light harvesting antenna complex. The standard linearized approximation, which truncates the phase of path integral for dynamical quantities to linear order in the difference between forward and backward paths, is a good approximation for short time propagation but can cause a serious problem for the long time calculations and, for example, it can lead to nonpositive definite populations. Moreover, the truncation of the dependence of the phase of the propagator in terms the mapping variable quantum subsystem degrees of freedom to linear order can result in inaccurate treatment of the dynamics even at shorter times especially for multilevel systems.

In this paper, we extend the iterative linearized density matrix (ILDMD) propagation approach¹ to model exciton transport processes in photosynthetic antenna complexes. The scheme uses a linearized approximation⁴⁴ for short time propagation segments, and concatenates these segments by Monte Carlo sampling. The approach is nonperturbative and does not require making the Markovian approximation, moreover, it does not require any particular form for the Hamiltonian, and thus can be applied to treat general system-bath interactions as well as arbitrary forms for the bath. The iterative scheme overcomes the linearized approximation for the environmental degrees of freedom by using it as a short time propagator that can be accurate for fairly long time segments. This is the only approximation in this method. The electronic degrees of freedom are described by mapping variables, the evolution of which, can be treated exactly without linearization.^{40,45,46} The approach is demonstrated in calculations on models of coherent exciton transfer in the Fenna–Matthews–Olsen (FMO) pigment-protein complex where detailed comparisons with other methods^{15,33,38} can be made.

II. METHOD

The ILDM propagation scheme^{1,47} assumes a quantum system represented by a number of discrete basis states $|n\rangle$ coupled to an environment described by continuous coordinates (\hat{R}, \hat{P}) , which can be highly dimensional. The approach outlined here is for a general time independent Hamiltonian written in a diabatic representation as

$$\hat{H} = \hat{P}^2/2M + \sum_{\lambda} h_{\lambda\lambda}(\hat{R})|\lambda\rangle\langle\lambda| + \sum_{\lambda < \lambda'} h_{\lambda\lambda'}(\hat{R})(|\lambda\rangle\langle\lambda'| + |\lambda'\rangle\langle\lambda|). \quad (1)$$

Following the work of various groups^{39–42} it is convenient to use the “mapping” representation where the quantum state population, $|\lambda\rangle\langle\lambda|$, and coherence, $|\lambda\rangle\langle\lambda'|$, operator terms are replaced by harmonic oscillator raising and lowering opera-

tors, and expressing these in terms of their oscillator coordinates and momenta $(\hat{q}_\alpha, \hat{p}_\alpha)$, the mapping variables, the exact Hamiltonian is rewritten in the form

$$\hat{H} = \hat{P}^2/2M + \frac{1}{2} \sum_{\lambda} h_{\lambda\lambda}(\hat{R}) (\hat{q}_{\lambda}^2 + \hat{p}_{\lambda}^2 - \hbar) + \frac{1}{2} \sum_{\lambda, \lambda'} h_{\lambda\lambda'}(\hat{R}) (\hat{q}_{\lambda} \hat{q}_{\lambda'} + \hat{p}_{\lambda} \hat{p}_{\lambda'}). \quad (2)$$

The density matrix is evolved by applying a sequence of combined forward-backward propagators. For two finite steps of duration t , for example, we have $\hat{\rho}(2t) = e^{-(i/\hbar)\hat{H}t} e^{-(i/\hbar)\hat{H}t} \hat{\rho}(0) e^{(i/\hbar)\hat{H}t} e^{(i/\hbar)\hat{H}t}$. Each forward and backward propagator pair is represented in terms of discrete (here k labels the time slice) phase space path integrals in the environmental variables, and double sums over quantum states.^{1,43} Our approach involves transforming to mean $\bar{R}_k = (R_k + R'_k)/2$ and difference $Z_k = (R_k - R'_k)$ paths in the environmental variables and expanding the action to linear order in the forward-backward path difference.^{48–52} The path integrals over the forward and backward mapping variables can be performed exactly^{44,45} using semiclassical trajectories in the forward $(q_{\lambda,k}, p_{\lambda,k})$, and backward $(q'_{\lambda,k}, p'_{\lambda,k})$ mapping variables as they appear quadratically in the Hamiltonian and the semiclassical approach is exact in this case. The approximation is thus to keep terms in the phase to linear order in the difference in environment variables but include all interference effects between the forward and backward paths of the quantum subsystem variables. This linearization in the bath degrees of freedom will be reliable if the propagation time t is sufficiently small. Alternatively, as outlined below, the linearized result can be used as a short time approximation and iterated to provide reliable results for longer times.

The final result of this linearized approach is a trajectory algorithm (detailed in Ref. 1) that can be summarize as follows. (1) Sum over forward and backward initial quantum states n_0 , and n'_0 , and select the final density matrix element of interest, n_t , and n'_t . (2) Sample mean environment path initial position \bar{R}_0 and momentum \bar{P}_1 from the Wigner distribution $[\hat{\rho}]_W^{n_0, n'_0}(\bar{R}_0, \bar{P}_1)$.⁵³ Propagate the environmental subsystem degrees of freedom using classical mechanics with the final state density matrix element dependent force

$$F_k^{n_t, n'_t} = -\frac{1}{2} \{ \nabla h_{n_t, n_t}(\bar{R}_k) + \nabla h_{n'_t, n'_t}(\bar{R}_k) \} - \frac{1}{2} \sum_{\lambda \neq n_t} \nabla h_{n_t, \lambda}(\bar{R}_k) c_{n_t, \lambda, k} - \frac{1}{2} \sum_{\lambda \neq n'_t} \nabla h_{n'_t, \lambda}(\bar{R}_k) c'_{n'_t, \lambda, k}, \quad (3)$$

with $c_{n_t, \lambda, k} = \{ (p_{n_t, k} p_{\lambda, k} + q_{n_t, k} q_{\lambda, k}) / (p_{n_t, k}^2 + q_{n_t, k}^2) \}$ and a similar expression in the primed (backward propagating) mapping variables. Auxiliary harmonic equations for the forward and backward mapping variables must be propagated to determine these quantities, this can be done analytically. (3) Finally, each trajectory's contribution to the density matrix is weighted by a complex factor $r_{t, n_t}(\{\bar{R}_k\}) r'_{t, n'_t}(\{\bar{R}_k\}) e^{-i\epsilon \sum_{k=1}^N (\theta_{n_t}(\bar{R}_k) - \theta_{n'_t}(\bar{R}_k))}$ involving functions

r_{t, n_t} and θ_{n_t} that depends on the mean path of the environment and contain the mapping variables, potentials, and couplings (see Ref. 1 for details). Here $\epsilon = t/N$. This approach can be iterated for multiple time segments t using an importance sampling Monte Carlo procedure that selects the most important density matrix elements at intermediate times controlling the exponentially diverging number of paths through state label space. The method has been bench marked against exact multiconfiguration time dependent Hartree (MCTDH) calculations for a variety of nonadiabatic reactive scattering, and condensed phase models,¹ and the approach gives reliable results for general Hamiltonians and requires comparable computation resources to other available methods for treating such models.

III. SYSTEM-BATH MODEL HAMILTONIAN

In this letter, we report results obtained using the ILDM propagation approach applied to models of the FMO complex^{14,30,32,33,38,54–60} that are formulated in terms of a dissipative exciton Hamiltonian that describes excitation energy transfer and relaxation in multichromophore systems. In these models each chromophore experiences dissipative interactions with its own independent bath thus the general Hamiltonian has the following form:

$$\hat{H}_{\text{indep}}^{\text{FMO}} = \sum_{\alpha=1}^{N_{\text{state}}} \left\{ \epsilon_{\alpha} + \sum_{l=1}^{n^{(\alpha)}} c_l^{(\alpha)} x_l^{(\alpha)} + \sum_{\beta=1}^{N_{\text{state}}^{n^{(\beta)}}} \sum_{m=1}^{n^{(\beta)}} \frac{1}{2} [p_m^{(\beta)2} + \omega_m^{(\beta)2} x_m^{(\beta)2}] \right\} \times |\alpha\rangle\langle\alpha| + \sum_{\alpha < \beta}^{N_{\text{state}}} \Delta_{\alpha, \beta} [|\alpha\rangle\langle\beta| + |\beta\rangle\langle\alpha|]. \quad (4)$$

The electronic Hamiltonian is determined by the diagonal electronic site energies, ϵ_{α} , of the chromophores, and the off-diagonal electronic couplings between the chromophores, $\Delta_{\alpha, \beta}$. The spectral densities $j^{(\alpha)}(\omega)$ for each chromophore's independent bath of bilinearly coupled harmonic oscillators are assumed to be identical for the different models studied here and they have either the Ohmic with Debye cutoff form or an Ohmic with exponential cutoff form.

For the Ohmic with Debye cutoff $j^{(\alpha)}(\omega) = j(\omega) = 2\lambda(\omega\tau_c) / [(\omega\tau_c)^2 + 1]$ is parameterized by a ‘‘solvent reorganization energy,’’ $\lambda = 1/\pi \int_0^{\infty} d\omega j(\omega)/\omega$, which controls the overall strength of the interaction between the quantum subsystem and the bath, and the bath relaxation time, τ_c , which controls the range of frequencies or time scales on which the bath can respond. With the Ohmic and exponential cutoff form on the other hand, $j(\omega) = (\lambda/\omega_c) \omega \exp[-\omega/\omega_c]$, the bath response is determined by the cutoff frequency ω_c . The system-bath bilinear coupling constants, $c_l^{(\alpha)}$, appearing in the Hamiltonian model are determined from these spectral densities using the definition $j^{(\alpha)}(\omega) = \pi/2 \sum_l^{n^{(\alpha)}} \times (c_l^{(\alpha)2}/\omega_l^{(\alpha)}) \delta(\omega - \omega_l^{(\alpha)})$.

IV. RESULTS

First, we consider some simplified two level system models^{32,38} whose parameters are chosen to mimic those expected in the FMO multistate excitation energy transfer system. The object of this study is to provide a basis to judge the

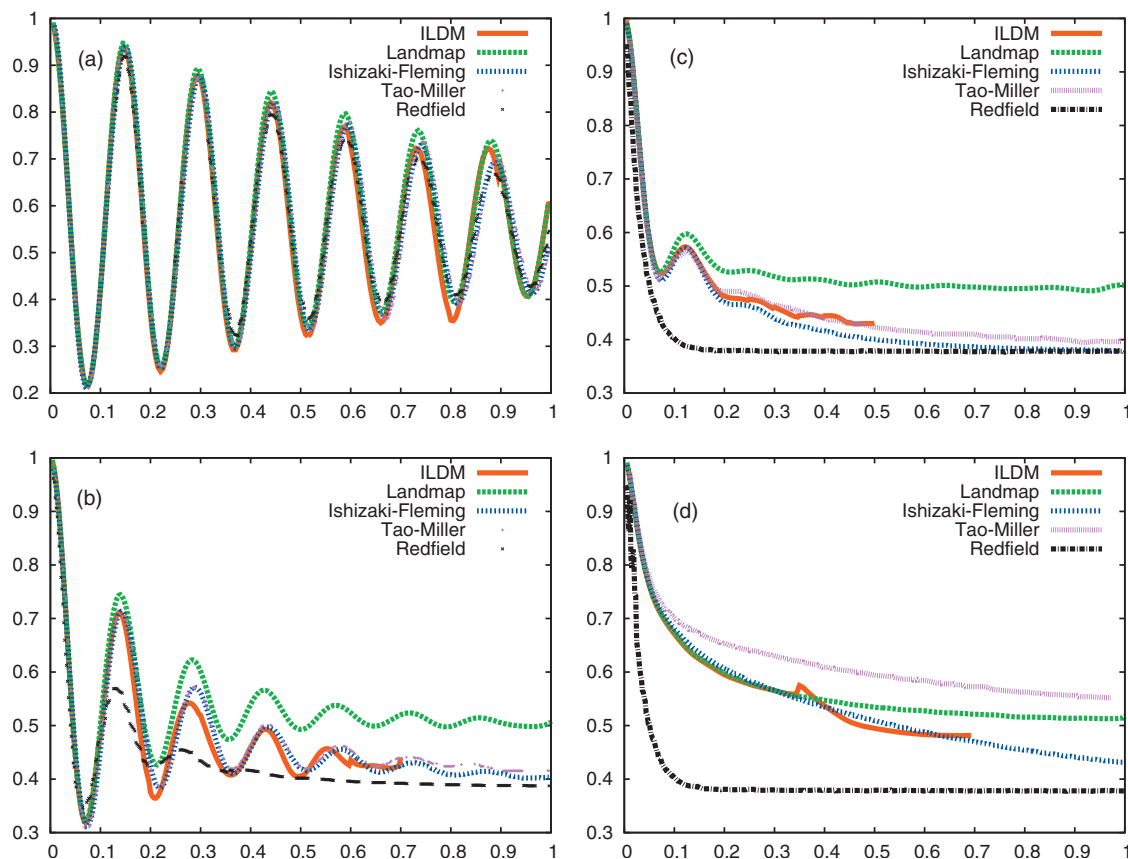


FIG. 1. Population of site 1 as a function of time (in ps) for a two state model (Ref. 32). Exciton state energy gap is $(\epsilon_1 - \epsilon_2) = 100 \text{ cm}^{-1}$, excitonic coupling is $\Delta_{1,2} = 100 \text{ cm}^{-1}$, temperature is $T = 300 \text{ K}$, characteristic time of the phonon bath is $\tau_c = 100 \text{ fs}$, and solvent reorganization energy is varied from $\lambda = 2 \text{ cm}^{-1}$ [panel (a)], $\lambda = 20 \text{ cm}^{-1}$ [panel (b)], $\lambda = 100 \text{ cm}^{-1}$ [panel (c)], and $\lambda = 500 \text{ cm}^{-1}$ [panel (d)]. Both the ILDM and Landmap results are calculated using the nonadiabatic dynamics theory outlined in this paper. Results labeled Tao–Miller were computed using the linearized semiclassical initial value representation theory and are taken from Ref. 38. Results labeled Ishizaki–Fleming were generated using the hierarchical coupled reduced master equation approach and are taken from Ref. 32 as were the results generated using Redfield theory.

reliability of results from various widely used, and recently developed approximate theoretical approaches capable of describing quantum coherence, as well as nonperturbative and non-Markovian effects. These comparative studies enable us to explore in detail the convergence of the ILDM propagation scheme for applications to model light harvesting systems. In the first model studied,^{32,38} the site energies are $\epsilon_1 = 100.0 \text{ cm}^{-1}$ and $\epsilon_2 = 0.0 \text{ cm}^{-1}$, the off-diagonal electronic coupling between the two states is $\Delta_{1,2} = 100.0 \text{ cm}^{-1}$, and we vary the solvent reorganization energy (measured here compared to the strength of the electronic coupling) through the wide range of values $\lambda = \Delta_{1,2}/50$, $\Delta_{1,2}/5$, $\Delta_{1,2}$, $5\Delta_{1,2}$, and consider two different limits for the solvent relaxation time, $\tau_c = 100 \text{ fs}$, and $\tau_c = 500 \text{ fs}$. In these first studies, the Ohmic with Debye cutoff spectral density is employed. The second model discussed below³³ involves a slightly different system with $\epsilon_1 = 0.0 \text{ cm}^{-1}$, $\epsilon_2 = 120.0 \text{ cm}^{-1}$, $\Delta_{1,2} = -87.0 \text{ cm}^{-1}$, and the bath spectral density in this second model has the Ohmic with exponential cutoff form, with fixed solvent reorganization energy of $\lambda = 50 \text{ cm}^{-1}$ (i.e., $\sim 0.6|\Delta_{1,2}|$), and $\omega_c = 50 \text{ cm}^{-1}$ (corresponding to $\tau_c = 106 \text{ fs}$). For this simplified model, we explore the temperature dependence in the range $T = 10\text{--}300 \text{ K}$. The second two state model with its initially occupied state 1 lower in energy than state 2 resembles more

closely the full seven state FMO model Hamiltonian^{14,33,38,53} that is used in later calculations.

In all studies, state 1 is initially occupied and the analytic solution for the bare two level system part of the problem gives that the initially occupied state population should behave as $|a_1(t)|^2 \sim 1 - 4 \cos^2 \theta \sin^2 \theta \sin^2(\delta t/\hbar)$ where $\delta = \frac{1}{2} \sqrt{[\epsilon_1 - \epsilon_2]^2 + 4\Delta_{1,2}^2}$ and $\theta = \frac{1}{2} \{ \pi/2 - \sin^{-1}([\epsilon_1 - \epsilon_2]/2\delta) \}$. The bare electronic subsystem for the first model, for example, should thus show state 1 population oscillations with a period of $\sim 149 \text{ fs}$, which dip down to a minimum of ~ 0.2 . This analytic solution should provide a reasonable approximation for the fully coupled system-bath problem in the limit of weak system-bath coupling and for sufficiently short times (compare with the results in Fig. 1 and 2).

The Redfield equation and theories based on it employ the perturbation theory (assuming that the system-bath (electron-phonon) coupling is small compared to other terms in the Hamiltonian) and then suppose that the memory kernel appearing in the resulting integrodifferential quantum master equation describing the dynamics of the reduced quantum system, decays rapidly compared to typical integration times of interest.^{31,61} This assumption enables the terms involving integrals out to time t appearing in the equation to be approximated by their integrals out to infinite time, reducing the integrodifferential form to a differential equation. This

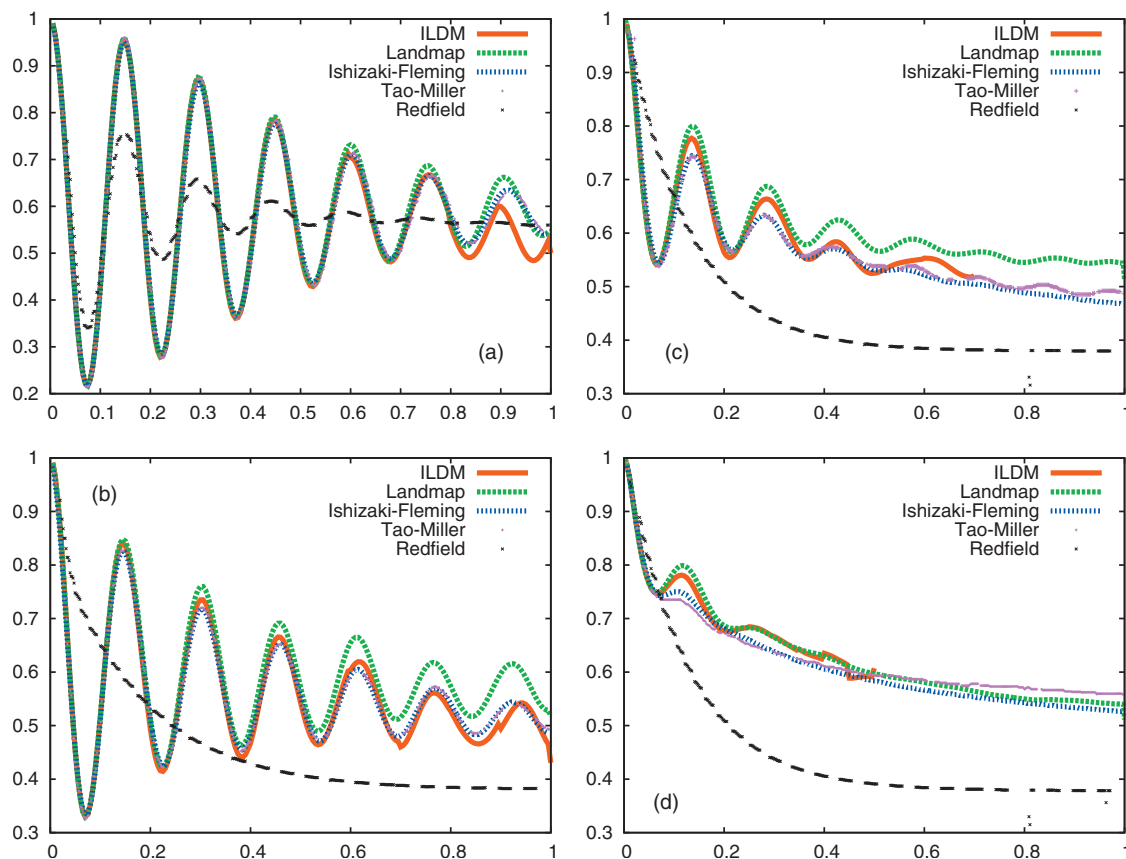


FIG. 2. Same as Fig. 1 except now the characteristic relaxation time for the phonon bath is $\tau_c=500$ fs.

second assumption is the Markovian approximation to the master equation that results in the final Redfield-like forms.^{31,60}

In Fig. 1, we display state population results obtained for a bath with a rapid solvent relaxation time, $\tau_c=100$ fs. With this value the bath memory kernel decays sufficiently rapidly to make the Markov approximation reliable and, provided the system-bath coupling perturbation (controlled by λ) is weak enough, the Redfield equation will give accurate results. This behavior is seen clearly in Fig. 1(a), corresponding to $\lambda=\Delta_{1,2}/50$, where the Redfield³² result is compared with various numerical solutions including the ILDM propagation scheme, the Landmap⁴⁴ approach that linearizes in only the bath degrees of freedom for the full time interval, the hierarchical coupled reduced master equation approach of Ishizaki and Fleming,³² and the fully linearized (both electronic mapping, and nuclear degrees of freedom) semiclassical initial value representation approach of Tao and Miller.³⁸ In this limit all theories capture the slow relaxation of the coherent beating as the exciton transfers between the two coupled chromophore sites. Increasing the system-bath coupling to $\lambda=\Delta_{1,2}/5$ [Fig. 1(b)] causes a break down of the time dependent perturbation theory underlying the Redfield equation and this results in its inability to capture the survival of the coherent population oscillations. Despite its inadequate description of the dynamics, the Redfield theory does, however, recover the asymptotic thermal equilibrium populations. The ILDM, full linearized SC-IVR, and hierarchical coupled reduced master equation approaches all cap-

ture the coherent oscillations at this intermediate-low coupling and agree quantitatively. The Landmap result captures the coherent oscillation characteristics but fails to give the thermal equilibrium asymptotic population correctly. In this approach the “action” in the density matrix propagator is truncated to linear order in the difference between forward and backward environmental paths while the forward and backward paths of the quantum subsystem variables are included explicitly. This gives rise to an accurate short time approximate propagator but if it is applied for longer full time intervals its accuracy degrades. The fully linearized SC-IVR approach (linearizing in both environment and quantum subsystem mapping variables) of Tao and Miller, on the other hand, is seen to generally perform reasonably well for this two level model, although its accuracy is poorer at higher friction as discussed below.

Increasing the solvent reorganization energy further to $\lambda=\Delta_{1,2}$, and $\lambda=5\Delta_{1,2}$ [Figs. 1(c) and 1(d), respectively] washes out the coherence in the Redfield result completely and gives a curve that seriously over estimates the excitation relaxation rate. The other approaches all predict significantly nonexponential relaxation with a fast component, some remnant oscillations at lower friction, and a long time tail. At the highest friction, the fully linearized SC-IVR result relaxes more slowly, whereas the Landmap agrees well with the ILDM and hierarchical coupled reduced master equation approaches out to about 300 fs before again relaxing to the wrong thermal equilibrium result. Curiously, the ILDM calculations are most difficult to converge in this limit of short

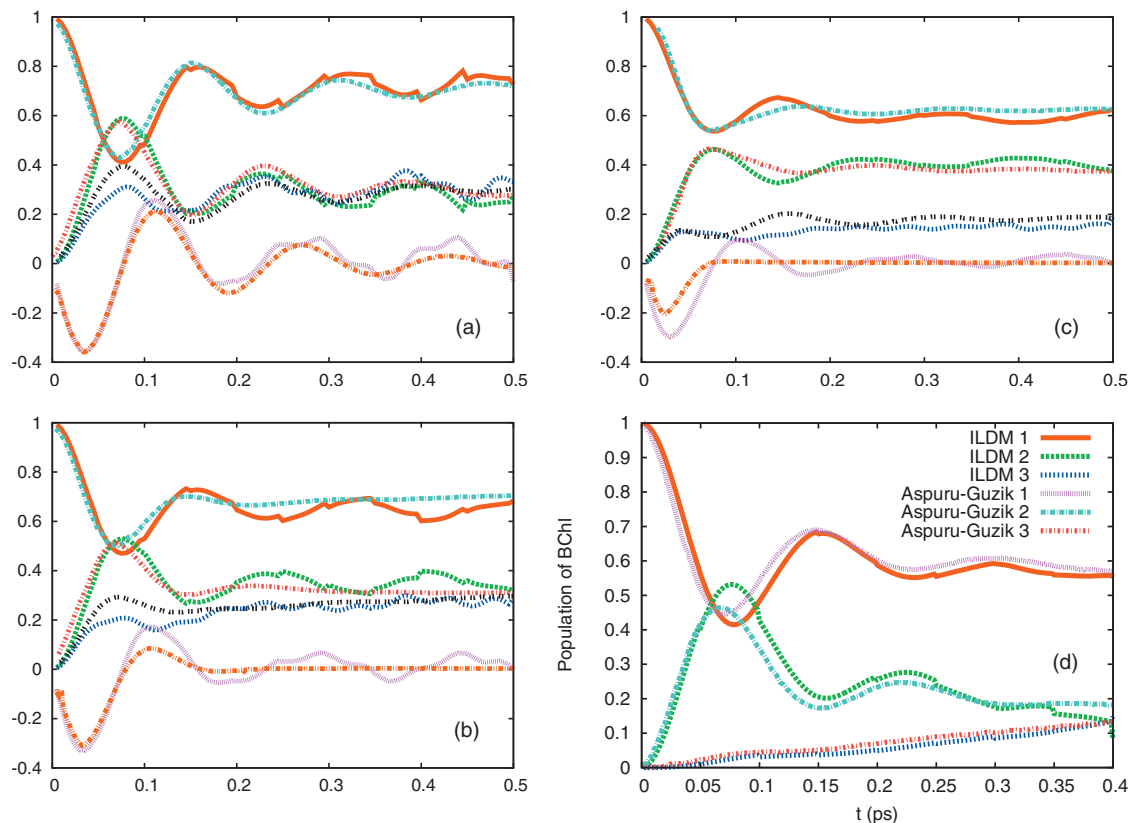


FIG. 3. Comparison of results from NMQJ and ILDM propagation calculations of populations and coherences for the second simplified two state model with $\epsilon_1=0.0$ cm⁻¹, $\epsilon_2=120.0$ cm⁻¹, and $\Delta_{1,2}=-87.0$ cm⁻¹. The bath spectral density has the Ohmic with exponential cutoff form with $\lambda=50$ cm⁻¹, and $\omega_c=50$ cm⁻¹. T=10 K, 77 K, and 300 K in panels (a), (b), and (c), respectively. In each panel, upper sets of curves (symmetric about 0.5) are populations, while progressively lower sets of curves are real and imaginary parts of coherence, respectively. Smoother curves in each case are NMQJ results and curves with more statistical noise are ILDM results. In these panels, x-axes give times in picoseconds. Panel (d) compares state populations computed with the NMQJ and the ILDM propagation approaches for the seven state FMO model (Refs. 14 and 33) with independent identical baths of exponentially truncated Ohmic form having $\lambda=35$ cm⁻¹ and $\omega_c=150$ cm⁻¹. The temperature for these FMO calculations is T=77 K.

bath relaxation time and strong system-bath coupling, hence the large jumps due to statistical noise at the time segment breaks. We find that under these conditions it is difficult to converge the ILDM approach with large numbers of smaller time segments. The result in the bottom right panel was obtained with only two segments (or hops). More segments give much larger noise in the results. Generally, however, the hierarchical coupled reduced master equation and ILDM propagation results are in good agreement over the wide range of friction values for this short relaxation time bath.

The time evolution of the site 1 population calculated with the various approaches for a bath with the much longer relaxation time of $\tau_c=500$ fs, and over the same range of λ values is presented in Fig. 2. In Fig. 2(a), we see that even at the lowest system-bath coupling where perturbation theory was reliable in the earlier results, the Redfield theory predicts very rapid damping of coherence due to the failure of the Markovian approximation for this long relaxation time bath. All the other approaches however are in good agreement recovering the transition from coherent to incoherent relaxation as the friction is increased in this more slowly responding environment. The Landmap approach again has difficulties reproducing the relaxation to equilibrium, although the deviation seems to be less here than with the faster bath. The Landmap approach, however, accurately captures the transition from coherent to incoherent relaxation, mimicking the

dynamics consistently reproduced by the ILDM, full linearized SC-IVR, and the hierarchical coupled reduced master equation approaches, but again the Landmap result tends to the wrong longtime limit. The fact that the Landmap result is more accurate for longer times also makes the convergence of the ILDM approach more easily achieved in this slow, strongly coupled bath compared to the results we observed for the fast bath displayed in Fig. 1.

As a final simplified model comparison in Fig. 3, panels (a)–(c) present states 1 and 2 populations, as well as the real and imaginary parts of the coherence, for the second two state model outlined above that uses the Ohmic spectral density with the exponential cutoff form. The figure compares results obtained employing the non-Markovian quantum jump (NMQJ)^{34,35} approach combined with the TCL equation developed by Reberstrost *et al.*³³ with those from ILDM calculations for T=10, 77, and 300 K, respectively. At the lowest temperature, the NMQJ approach gives results in good agreement with those from the ILDM calculations showing clear coherent beating of the populations. At higher temperatures, however, the NMQJ results show essentially no coherent population oscillations while the ILDM results suggest that for this model there are remnants of quantum coherent population and coherence oscillations even at T=300 K.

Figure 3(d) compares state populations computed with

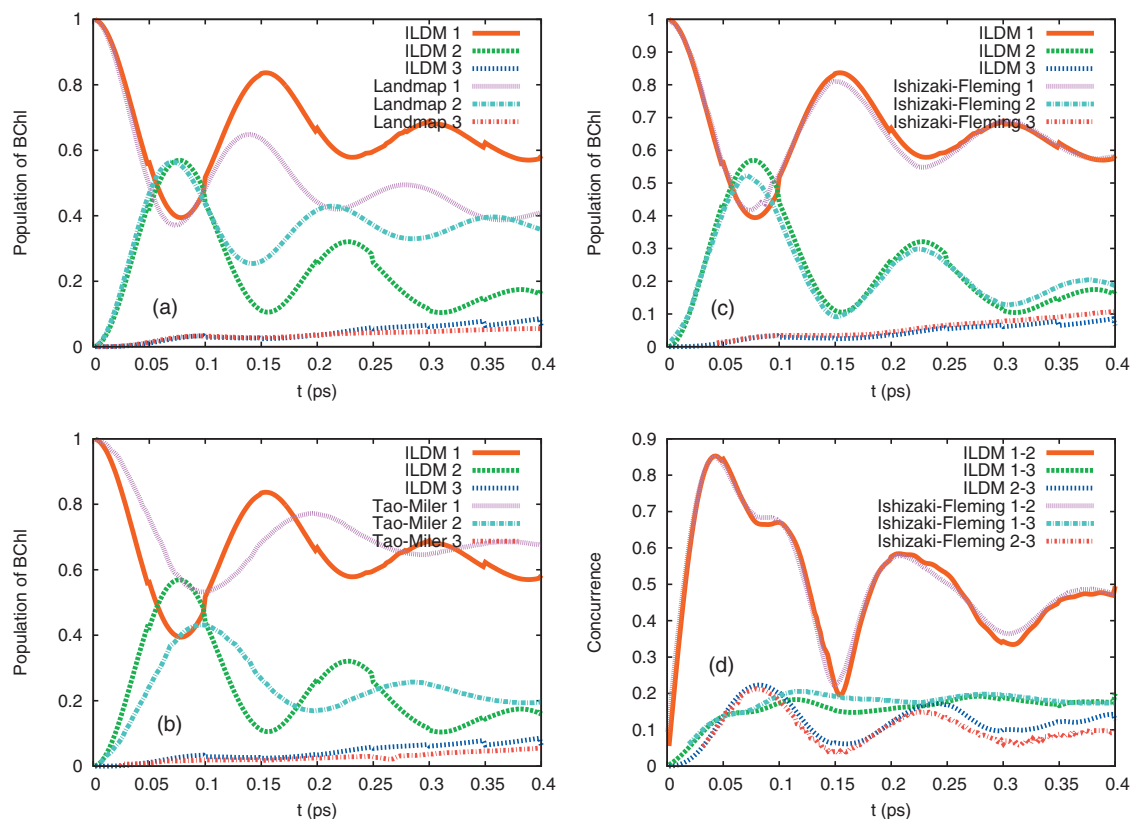


FIG. 4. Panels (a), (b), and (c) show populations as functions of time for the seven state model (Ref. 14) with $T=77$ K, and site 1 is initially occupied. For clarity, only states 1, 2, and 3 are plotted, although four states are included in the ILDM propagation and all seven states are included with the other propagation schemes. ILDM benchmark results are plotted for comparison in each panel. Panel (d) compares ILDM results for various concurrences $C_{i,j} = 2|\rho_{i,j}|$ with similar results obtained from the hierarchical reduced quantum master equation approach.

the NMQJ and the ILDM propagation approaches for a model that combines the seven state quantum subsystem model Hamiltonian of FMO presented in Refs. 14 and 33 with independent identical baths that are bilinearly coupled to each of the chromophores with the exponentially truncated Ohmic form having $\lambda=35$ cm^{-1} , and with $\omega_c=150$ cm^{-1} (corresponding to $\tau_c=35.3$ fs). The temperature for these calculations is $T=77$ K. As outlined below the ILDM results were obtained using a reduced Hamiltonian model including only four states. The results are in excellent agreement suggesting that the NMQJ approach is accurate for this multi-state problem under these conditions.

In the final set of studies reported here, the ILDM approach has been applied to explore the exciton dynamics and transfer pathway from initially excited chromophore 1 in the FMO complex using a reduced 4 state model employing only sites 1, 2, 3, and 4. The model Hamiltonian used in these studies includes all seven chromophore states¹⁴ but we truncate it only at the first four states visited by the dynamics starting at site 1. In the full model, the chromophore site energies span a 420 cm^{-1} range and the intersite electronic couplings range from 0 to 100 cm^{-1} . In these calculations, each chromophore interacts with its own independent, identical bath with a Debye truncated Ohmic spectral density form characterized by a fast solvent relaxation time $\tau_c=50$ fs and reorganization energy $\lambda=35$ cm^{-1} . These parameters put the model FMO system in the region where the Markovian approximation is expected to be reliable but the

moderately strong coupling makes the application of low order time dependent perturbation theory unsuitable.

In Fig. 4, the state populations obtained from these calculations are compared to the results from the various methods including: Landmap [panel (a)], full linearized SC-IVR [panel (b)], and the hierarchical coupled reduced master equation approach [panel (c)]. Figure 4(d) compares various coherence density matrix elements computed by ILDM and the hierarchical coupled reduced master equation approach.¹⁴ The comparison in panels (a) and (b) of the ILDM benchmark results with Landmap and full linearized SC-IVR results suggests that under these conditions the Landmap propagator is a significantly superior short time approximation compared to the LSC-IVR result.

The Landmap propagator gives results that agree accurately with those from the ILDM propagation out to about 100 fs, and the Landmap results show coherent oscillation that accurately lines up with the oscillations in the ILDM results. The amplitudes of the oscillations are well captured by the Landmap approach but the asymptotic populations are not accurately reproduced. With the full linearized SC-IVR result, the coherent oscillations damp out too quickly and their period is incorrect. This is surprising given the good performance observed for the reduced two state model discussed above. The fully linearized SC-IVR approach does seem to capture the asymptotic populations of the most important states involved in the dynamics reasonably reliably; however, this does come at a significant price. At longer

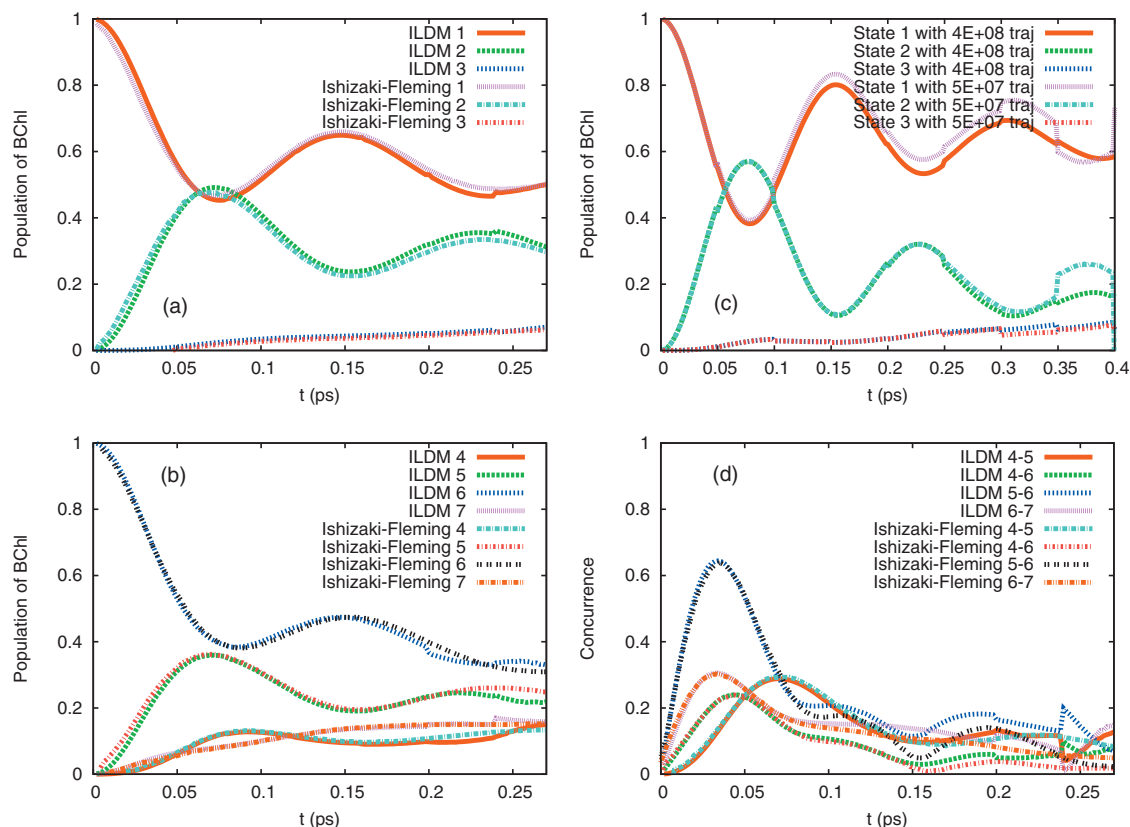


FIG. 5. Panels (a) and (b) show populations as functions of time for the seven state model (Ref. 14) with $T=300$ K and all propagations include dynamics of the full seven state Hamiltonian, although only the largest amplitude states are displayed for clarity. In panel (a), site 1 is initially occupied, while panel (b) presents results obtained with state 6 initially occupied. Panel (d) displays concurrence results ($C_{i,j}=2|\rho_{i,j}|$) obtained for the runs with $T=300$ K and state 6 initially occupied. In these three panels ILDM and hierarchical reduced quantum master equation results are compared. Panel (c) presents results exploring convergence of the ILDM calculations with ensemble sizes $N=5 \times 10^7$ trajectories, and $N=4 \times 10^8$. Results are obtained with $T=77$ K, and state 1 initially occupied.

times, the LSC-IVR results predict minor channel populations that are actually negative³⁸ as the approach does not guarantee unitarity of the full propagation. With the ILDM approach this problem is avoided provided sufficiently short segments and large enough numbers of iterations are used.

In Fig. 4(c) and 4(d), we see that the ILDM propagation results and those of the hierarchical coupled reduced master equation approach¹⁴ are in excellent agreement for both the population and coherence dynamics⁵⁴ at $T=77$ K. The results presented in the panels (a), (b), and (d) of Fig. 5 explore the influence of initial state on exciton energy transfer, and coherence dynamics using the full seven state model Hamiltonian. The results for ILDM and hierarchical coupled reduced master equation approaches are again in excellent agreement. As reported in the above results, when state 1 is initially occupied there are only three states involved in the dynamics: sites 1 and 2 exhibit long lived coherent superposition dynamics, while site 3 is fed population from this superposition state. From the results presented in Fig. 5(b), however, we see that when site 6 is initially excited the ensuing dynamics shows a coherent superposition of sites 6 and 5, which now feed amplitude to both states 4 and 7. The fact that pairs of states are coherently coupled in this pathway seems to provide a mechanism for more rapid excitation energy transfer away from the initially occupied site.

Finally in Fig. 5(c), we explore the convergence of our

ILDM calculations at $T=77$ K with ensemble size. As noted earlier the statistical uncertainty in our ensemble average results manifests itself in discontinuous jumps at the time segment breaks. These uncertainties grow at longer times but, as demonstrated in the figure, increasing the ensemble size by a factor of 40 in this example dramatically improves the statistical convergence even at longer times.

V. CONCLUSION

In this paper, we have shown that the ILDM propagation approach can accurately capture the coherent behavior of excitation energy transfer processes in complex systems and offers a computationally viable means of benchmarking quantum dynamics methods for large scale, non-Markovian, model systems at finite temperatures and for strong couplings (both electronic and environmental). For example, in the studies on realistic models of multichromophore photosynthetic light harvesting systems reported here, we demonstrated that widely used approximations for treating these systems such as those underlying Redfield theory and the master equation approaches built on it, are not useful in the context of photosynthetic light harvesting due to the breakdown of the Markovian approximation and the fact that the interactions are sufficiently strong in such problems to render low order perturbation theory unreliable. We have also used

the ILDM propagation approach to benchmark several recently proposed methods for treating systems where such approximations breakdown. In particular, we found that the hierarchical coupled reduced master equation approach¹⁴ and the non-Markovian quantum jump method³³ are capable of accurately treating the coherent quantum dynamics in a general class of system-bath models of excitation energy transfer in dissipative open quantum systems. The linearized semiclassical initial value representation approach³⁸ on the other hand, while providing an efficient and accurate method for treating two level model systems, runs into considerable difficulty when applied to multilevel quantum dissipative systems that seem to be the paradigm in light harvesting chromophore arrays. The Landmap approach,⁴⁴ which linearizes in the difference between the forward and backward paths of the environmental degrees of freedom while keeping interference effects between forward and backward paths of the mapping variables that describe the quantum subsystem, captures quantum coherence effects but has problems in some situations with reliably representing relaxation to equilibrium.

The dynamics displayed in Fig. 4(c) and 4(d) are ubiquitous for these sorts of multichromophore structures: when chromophore 1 is excited its population, and that of chromophore 2 to which it is coupled, show strong anticorrelated quantum beats. Simultaneously, the populations of this pair of coherently coupled states decay due to the coupling with the environment, and the coupling of chromophore 2 with chromophore 3 whose population shows subsequent steady growth resulting in the desired directional energy transfer function of the structure.

To help understand the effects of the environmental degrees of freedom on the short time dynamics of the different density matrix elements in Fig. 6, we overlay the plots of the populations [panel (b)] and coherences [plotted as the concurrence, $C_{i,j}=2|\rho_{i,j}|$, panel (a)] for the full system-bath model of FMO, with results obtained when the system-bath couplings are set to zero. The most obvious effect of the environmental coupling is to smear out the oscillatory features in this short time dynamics. The dynamics of the populations, however, show a more profound effect of the dissipation. In the presence of the bath coupling the populations of states 1 and 2 continue to beat against one another as they do without the environmental coupling present. However, we see that the coupling to the bath results in these two states losing amplitude, which begins to appear persistently in state 3. With no bath coupling, the state 3 population simply oscillates at small values and does not build up as is essential for functioning of the FMO complex as an excitonic diode that funnels excitation toward the reaction center adjacent to chromophore 3.^{14,55,57–60} Thus the right amount of excitonic dissipation to the protein environment is essential to promote effective energy transfer through the FMO complex. Too much dissipation would lead to localization and excessive energy loss before effective transfer to the reaction center.

To understand what influences the off-diagonal coherence density matrix elements, on the other hand, consider the full coupled system-bath wave function that has the form $|\Psi(t)\rangle = \sum_{\alpha} a_{\alpha}(t) \chi_{\alpha}(R, t) |\alpha\rangle$ in the site basis. The off-diagonal

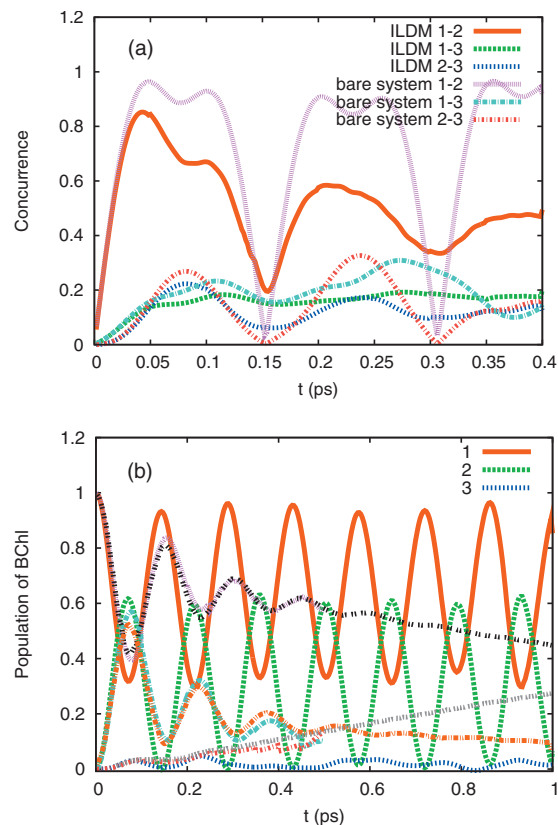


FIG. 6. Results explore the effect of coupling the model FMO excitonic quantum subsystem (Ref. 14) to its environment. Panel (b) presents populations as functions of time: red, green, and blue (oscillatory) curves give site populations starting with state 1 initially occupied in the absence of bath coupling. The other curves that show damped oscillations and long time linear growth (state 3) or decay (states 1 and 2) are computed with the full bath coupling included (ILDM and hierarchical reduced master equation results are presented). Panel (a) shows effect of removing the environment coupling on quantum subsystem coherences.

density matrix elements are written in terms of this system-bath wave function by projecting onto the site basis and integrating out the bath degrees of freedom according to the following result: $\rho_{\alpha,\beta}(t) = \int dR \langle \alpha | \Psi(t) \rangle \langle \Psi(t) | \beta \rangle = a_{\alpha}(t) a_{\beta}^{*}(t) \int dR \chi_{\alpha}(R, t) \chi_{\beta}^{*}(R, t)$. Thus the off-diagonal density matrix elements are determined by the time dependence of the site amplitudes $a_{\alpha}(t)$ for the different localized excitonic states, and the overlaps of the time dependent environmental wave packets $\chi_{\alpha}(R, t)$ that can be approximated as evolving under the influence of the different excitonic state potentials. In these expressions $R = (\{x_j^{(1)}\}, \dots, \{x_j^{(N_{\text{state}})}\})$ represents the positions of the oscillators (labeled with l running up to $n^{(\alpha)}$, for chromophore α) for each of the N_{state} independent baths associated with the different chromophores in the model Hamiltonian of Eq. (4).

The off-diagonal elements are thus affected by both amplitude transfer between the different coupled exciton states, and the nuclear wave packet overlap factor. To explore the influence of the overlap factor, we consider the following simplified model for the evolution of the environment in the presence of different quantum subsystem excitations. In this model, the bath is established initially in a thermal equilibrium state in which it is uncoupled from the quantum subsystem and, as the Hamiltonian is a sum of independent har-

monic terms, the initial nuclear wave packet state of a three chromophore systems for simplicity, can be written as $\chi(R, 0) = g^{(\alpha)}(\{x_i^{(\alpha)}\})g^{(\beta)}(\{x_i^{(\beta)}\})g^{(\gamma)}(\{x_i^{(\gamma)}\})$, where the functions $g^{(\alpha)}(\{x_i^{(\alpha)}\})$ are localized about the uncoupled bath equilibrium position characterized, for example, by $\{x_i^{(\alpha)} = 0\}$. The lowest order effect of the bilinear coupling between an exciton localized at site α and its environmental modes will arise from the displacement of the bath's equilibrium position. By completing the squares in the system-bath term in Eq. (4), it is easy to show that each oscillator's equilibrium displaces by $\Delta x_i^{(\alpha)} = c_i^{(\alpha)} / \omega_i^{(\alpha)2}$. We can thus approximate the evolved wave packets for the different exciton states at longer times as the environmental degrees of freedom tend to their new equilibrium positions as $\chi_\alpha(R, t \rightarrow \infty) = f^{(\alpha)}(\{x_i^{(\alpha)}\})g^{(\beta)}(\{x_i^{(\beta)}\})g^{(\gamma)}(\{x_i^{(\gamma)}\})$, $\chi_\beta^*(R, t \rightarrow \infty) = g^{(\alpha)*}(\{x_i^{(\alpha)}\})f^{(\beta)*}(\{x_i^{(\beta)}\})g^{(\gamma)*}(\{x_i^{(\gamma)}\})$, with a similar expression for χ_γ . Here the function $f^{(\alpha)}(\{x_i^{(\alpha)}\})$, for example, is localized about the coupled, excited system-bath equilibrium position $\{x_i^{(\alpha)} = \Delta x_i^{(\alpha)}\}$. The environmental wave packet overlap factor that modulates the off-diagonal coherence, $\rho_{\alpha,\beta}$, for example, will thus evolve as

$$\begin{aligned} \lim_{t \rightarrow \infty} \int dR \chi_\alpha(R, t) \chi_\beta^*(R, t) \\ = \int dx^{(\alpha)} f^{(\alpha)}(x^{(\alpha)}) g^{(\alpha)*}(x^{(\alpha)}) \\ \times \int dx^{(\beta)} g^{(\beta)}(x^{(\beta)}) f^{(\beta)*}(x^{(\beta)}) \\ \times \int dx^{(\gamma)} g^{(\gamma)}(x^{(\gamma)}) g^{(\gamma)*}(x^{(\gamma)}). \end{aligned} \quad (5)$$

Since the component packet for the γ chromophore bath experiences no differences in its interactions when the α or β chromophores are excited, the packets associated with these degrees of freedom essentially remain perfectly overlapped and do not modulate $\rho_{\alpha,\beta}$. We can get a simple estimate of the contributions to the overlap factor, $\int dR \chi_\alpha(R, t) \chi_\beta^*(R, t)$, from the displaced baths that interact with sites α and β . This estimate is influenced by the widths of the different bath wave functions, and the relative displacement between the equilibrium positions of the excited and unexcited system baths.

Combining the results in the last paragraph of Sec. III, it is easy to show that $(\pi/2) \sum_{i=1}^n c_i^{(\alpha)2} / \omega_i^{(\alpha)2} = \lambda$. Given a bath spectral density, $j(\omega)$, there are various equivalent ways to select a discrete set of frequencies and couplings that can be used in its representation.^{62–64} Independent of the precise details of this implementation, the above result suggests the following general relationship between the number of bath modes, their frequencies and couplings, and the solvent reorganization energy of the bath: $c_i^{(\alpha)} \sim \sqrt{\lambda/n^{(\alpha)}} \omega_i^{(\alpha)}$. To get an order of magnitude estimate of the overlap factor, we suppose that the component bath wave functions have product Gaussian forms thus, for example, $g^{(\alpha)} = \prod_{i=1}^n (a_i^{(\alpha)} / \pi)^{1/4} \exp[-a_i^{(\alpha)} x_i^{(\alpha)2} / 2]$ and $f^{(\alpha)} = \prod_{i=1}^n (a_i^{(\alpha)} / \pi)^{1/4} \exp[-a_i^{(\alpha)} (x_i^{(\alpha)} - \Delta x_i^{(\alpha)})^2 / 2]$. The component overlap then has the form

$\int dx^{(\alpha)} f^{(\alpha)} g^{(\alpha)*} = \prod_{i=1}^n \exp[-a_i^{(\alpha)} \Delta x_i^{(\alpha)2} / 4]$. From the above results, we find that $\Delta x_i^{(\alpha)2} \sim \lambda / (n^{(\alpha)} \omega_i^{(\alpha)2})$, and we can estimate the wave packet width from the shape of the thermal probability density suggesting the following value for the frequency dependent Gaussian parameter $a_i^{(\alpha)} = \omega_i^{(\alpha)} \tanh(\beta \hbar \omega_i^{(\alpha)} / 2) / \hbar$. Combining these results and using the fact that for our model the α and β baths have identical forms (each having n independent modes with the same frequency distribution), we obtain the long time limit for the overlap factor: $\lim_{t \rightarrow \infty} \int dR \chi_\alpha(R, t) \chi_\beta^*(R, t) \sim \exp[-(1/n) \sum_{i=1}^n (\lambda / 2 \hbar \omega_i) \tanh(\beta \hbar \omega_i / 2)]$. In the high temperature limit ($\beta = 1 / (k_B T) \rightarrow 0$), this overlap factor tends to $\exp[-\lambda \beta / 4]$, while at low temperatures we obtain $\lim_{T \rightarrow 0} \int dR \chi_\alpha(R, t) \chi_\beta^*(R, t) \sim \exp[-(1/n) \sum_{i=1}^n (\lambda / 2 \hbar \omega_i)]$. We note that with the system-bath model used here the overlap factor is in general independent of the number of bath oscillators used to represent the environment as the above exponents, involving terms such as $(1/n) \sum_{i=1}^n A(\omega_i)$, are simple averages over the distribution of bath oscillator frequencies and independent of the number of oscillators used to represent the dissipative environment.

The above analysis suggests that the overlap factor that controls the magnitude of the coherences will tend to a *constant* at long times, so for this independent harmonic bath model the coherences will *not* decay to zero unless the environmental coupling and temperature have appropriate values or the state amplitudes vanish. This occurs because of the localizing shifted harmonic forms used to describe the bath and system-bath interactions in these sorts of models. Sarovar *et al.*⁵⁴ have recently extended the hierarchical coupled reduced master equation approach, together with the full Hamiltonian model used here, to explore the long lived entanglement of the excitonic quantum subsystem in FMO with its protein environment described using precisely this bilinearly coupled harmonic model. Given the analysis presented here it is not surprising that these workers observe a very long time scale for the decoherence of the excitonic entanglement in this system with some coherences living significantly longer than 5 ps even at room temperature. In fact the off-diagonal density matrix elements corresponding to the states with populations that persist at long times show coherences that apparently plateau at finite values consistent with the analysis presented above.

This type of coherence behavior is to be contrasted with that treated by the theory of decoherence times presented by Prezhdo and Rossky.^{65,66} With their approach, the frozen Gaussian wave packets that are born as a result of nonadiabatic dynamics through coupling regions, modeled as linear diabatic potentials with constant forces, are driven apart by the forces arising from the different diabats, and so the wave packet overlap in the Prezhdo–Rossky model decays to zero. With the model analyzed above, on the other hand, the confining harmonic bath potentials mean that the bath wave packets moving on the different surfaces can't escape one another so their overlap does not vanish at long times and persistent coherence is observed with such models in con-

trast to the divergent wave packet evolution with the different linear surface model underlying the Prezhdo–Rossky theory.

We are currently exploring ways of extending the ILDM approach to longer times to explore the above finding of persistent coherence dynamics, as well as the appropriate choice of representation to understand this dynamics.^{47,67–70}

It will be particularly interesting to apply the ILDM approach to study the properties of different types of baths in relation to their decoherence and population transfer dynamics, for example, anharmonic baths, or baths that can represent long wavelength environmental modes that can cause correlated fluctuations in the energies of different sites that go beyond the independent bath model used in the study presented here. It will also be interesting to use these methods to explore bath models that have different spectral densities for the different excitonic states thus representing the possibility that chromophores couple to the environmental modes in different ways. Various schemes involving hierarchical bath models and partial reduced descriptions^{47,67,68} as well as employing different representations^{69,70} may be useful to improve the efficiency of the implementation of the ILDM approach for these studies. The mixed quantum-classical MD approach at the heart of the ILDM propagation scheme will, in principle, be applicable beyond the simple system-bath models considered here and fully atomistic simulations including anharmonicity, nonlinear couplings, and non-Markovian bath dynamics could be within reach with this scheme.

ACKNOWLEDGMENTS

We gratefully acknowledge support for this research from the National Science Foundation under Grant No. CHE-0911635. D.F.C. acknowledges the support of his Stokes Professorship in Nano Biophysics from Science Foundation Ireland. P.H. acknowledges the support of his MCC travel award from NSF and the hospitality of DFC during his visit to UCD. We also acknowledge a grant of supercomputer time from Boston University's Office of Information Technology and Scientific Computing and Visualization. Thanks Impy.

¹A. Damjanovic, F. Autenrieth, X. Hu, T. Ritz, and K. Schulten, *Q. Rev. Biophys.* **35**, 1 (2002).

²G. D. Scholes, *Annu. Rev. Phys. Chem.* **54**, 57 (2003).

³R. E. Fenna and B. W. Matthews, *Nature (London)* **258**, 573 (1975).

⁴A. Camara-Artigas, R. E. Blankenship, and J. P. Allen, *Photosynth. Res.* **75**, 49 (2003).

⁵J. L. Herek, N. J. Fraser, T. Pullerits, P. Martinsson, T. Polivka, H. Scheer, R. J. Cogdell, and V. Sundstrom, *Biophys. J.* **78**, 2590 (2000).

⁶M. A. Thompson, M. C. Zerner, and J. Fajer, *J. Phys. Chem.* **95**, 5693 (1991).

⁷J. A. Leegwater, *Prog. Biophys. Mol. Biol.* **65**, PE204 (1996).

⁸Y. F. Li, W. L. Zhou, R. E. Blankenship, and J. P. Allen, *J. Mol. Biol.* **271**, 456 (1997).

⁹N. Makri, E. J. Sim, D. E. Makarov, and M. Topaler, *Proc. Natl. Acad. Sci. U.S.A.* **93**, 3926 (1996).

¹⁰E. Sim and N. Makri, *J. Phys. Chem. B* **101**, 5446 (1997).

¹¹S. Savikhin, D. R. Buck, and W. S. Struve, *Chem. Phys.* **223**, 303 (1997).

¹²G. S. Engel, T. R. Calhoun, E. L. Read, T.-K. Ahn, T. Mancal, Y.-C. Cheng, R. E. Blankenship, and G. R. Fleming, *Nature (London)* **446**, 782 (2007).

¹³H. Lee, Y.-C. Cheng, and G. R. Fleming, *Science* **316**, 1462 (2007).

¹⁴A. Ishizaki and G. R. Fleming, *Proc. Natl. Acad. Sci. U.S.A.* **106**, 17255 (2009).

¹⁵E. Collini, C. Y. Wong, K. E. Wilk, P. M. G. Curmi, P. Brumer, and G. D. Scholes, *Nature* **463**, 644 (2010).

¹⁶G. D. Scholes, *J. Phys. Chem. Lett.* **1**, 2 (2010).

¹⁷S. Jang, M. D. Newton, and R. J. Silbey, *Phys. Rev. Lett.* **92**, 218301 (2004).

¹⁸S. Jang, M. D. Newton, and R. J. Silbey, *J. Phys. Chem. B* **111**, 6807 (2007).

¹⁹Y.-C. Cheng and R. J. Silbey, *Phys. Rev. Lett.* **96**, 028103 (2006).

²⁰C. P. Hsu, G. R. Fleming, M. Head-Gordon, and T. Head-Gordon, *J. Chem. Phys.* **114**, 3065 (2001).

²¹R. Métivier, F. Nolde, K. Muellen, and T. Basché, *Phys. Rev. Lett.* **98**, 047802 (2007).

²²D. J. Heijs, V. A. Malyshev, and J. Knoester, *Phys. Rev. Lett.* **95**, 177402 (2005).

²³M. Schröder, U. Kleinekathofer, and M. Schreiber, *J. Chem. Phys.* **124**, 084903 (2006).

²⁴S. Jang, *J. Chem. Phys.* **127**, 174710 (2007).

²⁵S. Jang, M. D. Newton, and R. J. Silbey, *J. Chem. Phys.* **118**, 9312 (2003).

²⁶S. Jang and R. J. Silbey, *J. Chem. Phys.* **118**, 9324 (2003).

²⁷A. Olaya-Castro, C. Fan-Lee, F. Fassioli-Olsen, and N. F. Johnson, *Phys. Rev. B* **78**, 085115 (2008).

²⁸X. J. Yang, T. E. Dykstra, and G. D. Scholes, *Phys. Rev. B* **71**, 045203 (2005).

²⁹M. N. Yang, *J. Chem. Phys.* **123**, 124705 (2005).

³⁰B. Palmieri, D. Abramavicius, and S. Mukamel, *J. Chem. Phys.* **130**, 204512 (2009).

³¹A. Ishizaki and G. R. Fleming, *J. Chem. Phys.* **130**, 234110 (2009).

³²A. Ishizaki and G. R. Fleming, *J. Chem. Phys.* **130**, 234111 (2009).

³³P. Rebentrost, R. Chakraborty, and A. Aspuru-Guzik, *J. Chem. Phys.* **131**, 184102 (2009).

³⁴J. Piilo, S. Maniscalco, K. Häkönen, and K.-A. Suominen, *Phys. Rev. Lett.* **100**, 180402 (2008).

³⁵J. Piilo, K. Häkönen, S. Maniscalco, and K.-A. Suominen, *Phys. Rev. A* **79**, 062112 (2009).

³⁶S. Jang, Y.-C. Cheng, D. R. Reichman, and J. D. Eaves, *J. Chem. Phys.* **129**, 101104 (2008).

³⁷S. Jang, *J. Chem. Phys.* **131**, 164101 (2009).

³⁸G. Tao and W. H. Miller, *J. Phys. Chem. Lett.* **1**, 891 (2010).

³⁹H.-D. Meyer and W. H. Miller, *J. Chem. Phys.* **70**, 3214 (1979).

⁴⁰G. Stock and M. Thoss, *Phys. Rev. Lett.* **78**, 578 (1997).

⁴¹X. Sun and W. H. Miller, *J. Chem. Phys.* **106**, 6346 (1997).

⁴²M. Thoss and G. Stock, *Phys. Rev. A* **59**, 64 (1999).

⁴³E. R. Dunkel, S. Bonella, and D. F. Coker, *J. Chem. Phys.* **129**, 114106 (2008).

⁴⁴S. Bonella and D. F. Coker, *J. Chem. Phys.* **122**, 194102 (2005).

⁴⁵S. Bonella and D. F. Coker, *J. Chem. Phys.* **118**, 4370 (2003).

⁴⁶S. Bonella and D. F. Coker, *J. Chem. Phys.* **114**, 7778 (2001).

⁴⁷P. Huo, S. Bonella, L. Chen, and D. F. Coker, *Chem. Phys.* **370**, 87 (2010).

⁴⁸R. Hernandez and G. A. Voth, *Chem. Phys.* **233**, 243 (1998).

⁴⁹J. A. Poulsen, G. Nyman, and P. J. Rossky, *J. Chem. Phys.* **119**, 12179 (2003).

⁵⁰Q. Shi and E. Geva, *J. Phys. Chem. A* **107**, 9059 (2003).

⁵¹H. Wang, X. Sun, and W. H. Miller, *J. Chem. Phys.* **108**, 9726 (1998).

⁵²M. F. Herman and D. F. Coker, *J. Chem. Phys.* **111**, 1801 (1999).

⁵³Z. Ma and D. F. Coker, *J. Chem. Phys.* **128**, 244108 (2008).

⁵⁴M. Sarovar, A. Ishizaki, G. R. Fleming, and K. B. Whaley, *Nat. Phys.* **6**, 462 (2010).

⁵⁵J. Adolphs and T. Renger, *Biophys. J.* **91**, 2778 (2006).

⁵⁶M. Cho, H. M. Vaswani, T. Brixner, J. Stenger, and G. R. Fleming, *J. Phys. Chem. B* **109**, 10542 (2005).

⁵⁷R. J. W. Louwe, J. Vrieze, A. J. Hoff, and T. J. Aartsma, *J. Phys. Chem. B* **101**, 11280 (1997).

⁵⁸T. Renger and V. May, *J. Phys. Chem. A* **102**, 4381 (1998).

⁵⁹S. I. E. Vulto, M. A. de Baat, R. J. W. Louwe, H. P. Permentier, T. Neef, M. Miller, H. van Amerongen, and T. J. Aartsma, *J. Phys. Chem. B* **102**, 9577 (1998).

⁶⁰M. Wendling, M. A. Przyjalowski, D. Gülen, S. I. E. Vulto, T. J. Aartsma, R. van Grondelle, and H. van Amerongen, *Photosynth. Res.* **71**, 99 (2002).

- ⁶¹ Y. C. Cheng and R. J. Silbey, *J. Phys. Chem. B* **109**, 21399 (2005).
- ⁶² N. Makri, *J. Phys. Chem. B* **103**, 2823 (1999).
- ⁶³ H. Wang, M. Thoss, K. L. Sorge, R. Gelabert, X. Giménez, and W. H. Miller, *J. Chem. Phys.* **114**, 2526 (2001).
- ⁶⁴ D. Mac Kernan, G. Ciccotti, and R. Kapral, *J. Chem. Phys.* **116**, 2346 (2002).
- ⁶⁵ O. V. Prezhdo and P. J. Rossky, *J. Chem. Phys.* **107**, 5863 (1997).
- ⁶⁶ O. V. Prezhdo and P. J. Rossky, *Phys. Rev. Lett.* **81**, 5294 (1998).
- ⁶⁷ K. H. Hughes, C. D. Christ, and I. Burghardt, *J. Chem. Phys.* **131**, 024109 (2009).
- ⁶⁸ D. F. Coker, L. Chen, P. Huo, and S. Bonella, in *Multidimensional Quantum Mechanics with Trajectories*, edited by D. Shalashilin and M. P. de Miranda (CCP6, Daresbury, 2008), p. 165.
- ⁶⁹ M. S. Causo, G. Ciccotti, D. Montemayor, S. Bonella, and D. F. Coker, *J. Phys. Chem. B* **109**, 6855 (2005).
- ⁷⁰ S. Bonella and D. F. Coker, in *Quantum Dynamics of Complex Molecular Systems*, Lectures in Chemical Physics Vol. 83, edited by D. Micha and I. Burghardt (Springer, Berlin, 2006), p. 321.